Influence of boiling initiation surface superheat on subcooled water flow boiling critical heat flux in a SUS304 circular tube at high liquid Reynolds number

Hata, Koichi

Fukuda, Katsuya

Masuzaki, Suguru

(Citation)
International Journal of Heat and Mass Transfer,98:299-312

(Issue Date)
2016-07

(Resource Type)
journal article

(Version)
Accepted Manuscript

INFLUENCE OF BOILING INITIATION SURFACE SUPERHEAT ON SUBCOOLED WATER FLOW BOILING CRITICAL HEAT FLUX IN A SUS304 CIRCULAR TUBE AT HIGH LIQUID REYNOLDS NUMBER

Koichi Hata*

Graduate School of Maritime Sciences, Kobe University

5-1-1, Fukae-minami, Higashinada, Kobe 658-0022, Japan

hatako1@people.kobe-u.ac.jp

Katsuya Fukuda

Graduate School of Maritime Sciences, Kobe University

5-1-1, Fukae-minami, Higashinada, Kobe 658-0022, Japan

fukuda@maritime.kobe-u.ac.jp

Suguru Masuzaki

National Institute for Fusion Science

322-6 Oroshi-cho, Toki, Gifu 509-5292, Japan

masuzaki@LHD.nifs.ac.jp

ABSTRACT

* Corresponding author

The subcooled boiling heat transfer and the steady-state critical heat flux (CHF) in a vertical circular tube for the liquid Reynolds numbers (Re_d=3.65×10^4 to 3.08×10^5) and the flow velocities (u=3.95 to 30.80 m/s) were systematically measured by the experimental water loop comprised of a multistage canned-type circulation pump with high pump head. The SUS304 test tube of inner diameter (d=6 mm) and heated length (L=59.5 mm) was used in this work. The boiling initiation noise of outer surface of the test tube in the open air was simultaneously measured up to CHF point by the sound level meter (SLM) and the microphone of a video camera (MP). The outer surface temperatures of the SUS304 test tube with heating were also observed by an infrared thermal imaging camera (ITIC) and the color temperatures of outer surface of the test tube in the open air were observed by a video camera (VC). The subcooled boiling heat transfer and CHF for SUS304 circular tube were compared with the values calculated by authors' and other reseachers' correlations for the subcooled flow boiling heat transfer. The influences of flow velocity on the boiling initiation surface heat flux, the boiling initiation surface superheat, the subcooled boiling heat transfer and the CHF were investigated into details based on the experimental data. At the flow velocities higher than 13.3 m/s, boiling initiation surface heat fluxes were close to the CHFs and surface superheats at the CHF were over to the homogeneous spontaneous nucleation temperature as well as the lower limit of the heterogeneous spontaneous nucleation temperature. The dominant mechanism of the subcooled water flow boiling CHF on the SUS304 circular tube was discussed at high liquid Reynolds number.

KEYWORDS

Boiling Initiation Surface Superheat, Subcooled Water Flow Boiling, Critical Heat Flux, SUS304 Circular Tube, High Liquid Reynolds Number, Mechanism of CHF

1. INTRODUCTION

The knowledge of boiling initiation surface heat flux and surface superheat at high liquid Reynolds number is important to discuss the mechanism of critical heat flux (CHF) in a vertical circular tube. Many researchers have experimentally studied the steady-state CHFs uniformly heated on the normal tubes by a steadily increasing current for high liquid Reynolds number and have given the correlations for calculating CHFs on the normal tubes. It has been supposed that flow velocity will affect the boiling initiation surface heat flux and surface superheat, and the nucleate boiling heat transfer up to the CHF. Boiling initiation surface heat flux and surface superheat may shift to a very high value at higher flow velocity and a direct transition to film boiling or a trend of a decrease in CHF with an increase in the flow velocity may occur due to the heterogeneous spontaneous nucleation. The accurate measurement for the subcooled boiling heat transfer up to the CHF is necessary to clarify a change in the mechanism of CHF.

The turbulent heat transfer coefficients for the flow velocities (u=4.0 to 41.07 m/s), the inlet liquid temperatures (T_{in}=296.5 to 353.4 K), the inlet pressures (P_{in}=810.4 to 1044.2 kPa) and the increasing heat inputs ($Q=Q_0\,exp(t/\tau)$, τ=6.04 to 33.3 s) have been systematically measured by an experimental water loop. The VERTICAL Platinum test tubes of inner diameters (d=3, 6 and 9 mm), heated lengths (L=32.7 to 100 mm), ratios of heated length to inner diameter (L/d=5.51 to 33.3) and wall thickness (δ=0.3, 0.4 and 0.5 mm) with surface roughness (Ra=0.40 to 0.78 μm) were used. The influences of Reynolds number (Re_d), Prandtl number (Pr), dynamic viscosity (μ_l) and L/d on the turbulent heat transfer were investigated into details and, the widely and precisely predictable correlation of the turbulent heat transfer for heating of water in a vertical circular tube was given based on the experimental data [1, 2].

$$Nu_d = 0.02 Re_d^{0.85} Pr^{0.4} \left(\frac{L}{d}\right)^{-0.08} \left(\frac{\mu_l}{\mu_w}\right)^{0.14} \tag{1}$$

All properties in the equation are evaluated at the liquid bulk mean temperature, T_L [=(T_{in}+ $(T_{out})_{cal}$)/2], except μ_w, which is evaluated at the heater inner surface temperature. The correlation can describe the turbulent heat transfer coefficients obtained for the wide range of the temperature differences between average inner surface temperature and liquid bulk mean temperature (ΔT_L=5 to 140 K) with d=3, 6 and 9 mm, L=32.7 to 100 mm and u=4.0 to 41.07 m/s within ±15 % differences.

For many years the steady-state CHFs have been already measured by exponentially increasing heat input ($Q_0\, exp(t/\tau)$, τ=8.5 to 33.3 s) for the VERTICAL SUS304 test tube with the wide range of experimental conditions such as inner diameters (d=2 to 12 mm), heated lengths (L=22 to 149.7 mm), L/d (=4.08 to 74.85), outlet pressures (P_{out}=159 kPa to 1.1 MPa) and flow velocities (u=4.0 to 42.4 m/s) to establish the database for designing the divertor of the LHD [3-17]. And furthermore, we have given the steady-state CHF correlations against outlet and inlet subcoolings based on the effects of test tube inner diameter (d), flow velocity (u), outlet and inlet subcoolings ($\Delta T_{sub,out}$ and $\Delta T_{sub,in}$) and ratio of heated length to inner diameter (L/d) on CHF.

Outlet subcooling:

$$Bo_{cr} = 0.082 D^{*-0.1} We^{-0.3} \left(\frac{L}{d}\right)^{-0.1} Sc^{0.7} \qquad \text{for } \Delta T_{sub,out} \geq 30 \text{ K and } u \leq 13.3 \text{ m/s [3]} \qquad (2)$$

$$Bo_{cr} = 0.0523 D^{*-0.15} We^{-0.25} \left(\frac{L}{d}\right)^{-0.1} Sc^{0.7} \qquad \text{for } \Delta T_{sub,out} \geq 30 \text{ K and } u > 13.3 \text{ m/s [11]} \qquad (3)$$

Inlet subcooling:

$$Bo_{cr} = C_1 D^{*-0.1} We^{-0.3} \left(\frac{L}{d}\right)^{-0.1} e^{-\frac{(L/d)}{C_2 Re_d^{0.4}}} Sc^{*C_3} \qquad \text{for } \Delta T_{sub,in} \geq 40 \text{ K and } u \leq 13.3 \text{ m/s [4, 7]} \qquad (4)$$

$$Bo_{cr} = C_4 D^{*-0.15} We^{-0.25} \left(\frac{L}{d}\right)^{-0.1} e^{-\frac{(L/d)}{C_5 Re_d^{0.5}}} Sc^{*C_6} \qquad \text{for } \Delta T_{sub,in} \geq 40 \text{ K and } u > 13.3 \text{ m/s [11]} \qquad (5)$$

where C_1=0.082, C_2=0.53 and C_3=0.7 for L/d≤around 40 [4] and C_1=0.092, C_2=0.85 and C_3=0.9 for L/d>around 40 [7]. C_4=0.0523, C_5=0.144 and C_6=0.7 for L/d≤around 40 and C_4=0.0587, C_5=0.231 [11] and C_6=0.9 for L/d>around 40 [11]. Bo_{cr}, D^*, We, Sc and Sc^* are boiling number ($=q_{cr,sub}/Gh_{fg}$), non-dimensional diameter [$D^*=d/\{\sigma/g/(\rho_l-\rho_g)\}^{0.5}$], Weber number ($=G^2d/\rho_l\sigma$), non-dimensional outlet subcooling ($=c_{pl}\Delta T_{sub,out}/h_{fg}$) and non-dimensional inlet subcooling ($Sc^*=c_{pl}\Delta T_{sub,in}/h_{fg}$), respectively. Saturated thermo-physical properties were evaluated at the outlet pressure. Most of the data for the exponentially increasing heat input ($Q_0\ exp(t/\tau)$, τ=8.5 to 33.3 s, 3323 points) are within ±15 % differences of Eqs. (2), (3), (4) and (5) for the flow velocities, u, ranging from 4.0 to 42.4 m/s, respectively.

The objectives of present study are six fold. First is to measure the subcooled boiling heat transfer and the steady-state CHFs for a SUS304-circular test tube with the wide ranges of inlet subcoolings ($\Delta T_{sub,in}$= 141.35 to 159.03 K) and flow velocities (u=3.95 to 30.80 m/s) at high liquid Reynolds number (Re_d=3.65×10^4 to 3.08×10^5). Second is to measure simultaneously the boiling initiation noise of outer surface of the test tube in the open air up to CHF point by the sound level meter (SLM) and the microphone of a video camera (MP). Third is to observe the outer surface temperature of the SUS304-circular test tube with heating by an infrared thermal imaging camera (ITIC). Fourth is to observe the color temperatures of outer surface of the test tube in the open air by a video camera (VC). Fifth is to compare the surface heat fluxes, the inner surface temperatures and the outer ones of the SUS304-circular test tube calculated by the steady one-dimensional heat conduction equation with these SLM data, MP ones, ITIC ones and VC ones taken at the same time for the flow velocities ranging from 3.95 to 30.80 m/s, respectively. Sixth is to discuss the mechanism of the subcooled flow boiling critical heat flux in a vertical circular tube at high liquid Reynolds number based on the experimental data.

2. EXPERIMENTAL APPARATUS AND METHOD

The schematic diagram of experimental water loop comprised of the pressurizer is shown in Fig. 1. The loop is made of SUS304 stainless steel and is capable of working up to 2 MPa. The loop has five test sections whose inner diameters are 2, 3, 6, 9 and 12 mm. Test sections were vertically oriented with water flowing upward. The test section of the inner diameter of 6 mm was used in this work. The circulating water was distilled and deionized with about 20 μS/m specific resistivity. The circulating water through the loop was heated or cooled to keep a desired inlet temperature by pre-heater or cooler. The flow velocity was measured by a mass flow meter using a vibration tube (Nitto Seiko, CLEANFLOW 63FS25, Flow range=100 and 750 kg/min). The mass velocity was controlled by regulating the frequency of the three-phase alternating power source to the canned type circulation pump (Nikkiso Co., Ltd., Non-Seal Pump Multi-stage Type VNH12-C4 C-3S7SP, pump flow rate=12 m^3/h, pump head=250 m) with an inverter installed a 4-digit LED monitor (Mitsubishi Electric Corp., Inverter, Model-F720-30K). The pump input frequency shows the net pump input power and pump discharge pressure free of slip loss. The water was pressurized by saturated vapor in the pressurizer in this work. The pressure at the outlet of the test tube was controlled within ±1 kPa of a desired value by using a heater controller of the pressurizer.

The cross-sectional view of 6-mm inner diameter test section used in this work is shown in Fig. 2. The SUS304 test tube for the test tube inner diameter, d, of 6 mm, the heated length, L, of 59.5 mm with the commercial finish of inner surface was used in this work. Wall thickness of the test tube, δ, was 0.5 mm. Four fine 0.07-mm diameter platinum wires were spot-welded on the outer surface of the 6 mm inner diameter test tube as potential taps: the first one is at the position of 4.6 mm from the leading edge of the test tube, and the second to forth ones are at 16.5, 16.8 and 15.7 mm from the previous ones, respectively, for the test tube number of THD-F191. The effective length, L_{eff}, of the 6 mm inner diameter test tube between the first potential tap and forth one on which average heat transfer was measured was 49.0 mm. The silver-coated 5-mm thickness copper-electrode-plates to supply heating current were soldered to the surfaces of the both ends of the test tube. The both ends of test tube were electrically isolated from the loop by Bakelite plates of 14-mm thickness. The inner surface condition of the test tube was observed by the scanning electron microscope (SEM) photograph (JEOL JXA8600) and inner surface roughness was measured by Tokyo Seimitsu Co., Ltd.'s surface texture measuring instrument (SURFCOM 120A). Figure 3 shows the SEM photograph of the SUS304 test tube for d=6 mm with commercial finish of inner surface. The values of inner surface roughness for Ra, $Rmax$ and Rz were measured 3.89, 21.42 and 15.03 μm, respectively.

The SUS304 test tube has been heated with an exponentially increasing heat input supplied from a direct current source (Takasago Ltd., NL035-500R, DC 35 V-3000 A) through the two copper electrodes shown in Fig. 4. Heat transfer processes caused by exponentially increasing heat inputs, $Q_0\ exp(t/\tau)$, were measured for the SUS304 test tube. The exponential periods, τ, of the heat input ranged from 7.02 to 8.51 s. The common specifications of the direct current source are as follows. Constant-voltage (CV) mode regulation is a 4.75 mV minimum, CV mode ripple is 500 μV r.m.s. or better and CV mode transient response time is less than 200 μsec (Typical) against 5 % to full range change of load. The boiling initiation noise of outer surface of the test tube in the open air was simultaneously measured up to CHF point by the sound level meter (SLM, RION CO., LTD. Sound Level Meter NL-42) and the microphone of a video camera (MP, SONY Handycam HDR-CX270V). The outer surface temperature of the test tube with heating was observed by an infrared thermal imaging camera (ITIC, NEC Avio Infrared Technologies Co., Ltd. Thermography TVS-200EX) and the color temperature of outer surface of the test tube in the open air was observed by a video camera (VC, SONY Handycam HDR-CX270V). The accuracy of an infrared thermal imaging camera (ITIC) is ±2 % of reading. The outer surface of the test tube was uniformly painted black with black body spray (Japan Sensor Corporation, JSC-3, emissivity, ε, of 0.94) in this work.

The average temperature, $\overline{T}$, of the SUS304 test tube shown in Fig. 4 was measured with resistance thermometry participating as a branch of a double bridge circuit for the temperature measurement. The output voltages from the bridge circuit, V_T, together with the voltage drop across the potential taps of the test tube (first and forth potential taps, $V_R=IR_T$, first and second ones, $V_{R1}=IR_{T1}$, second and third ones, $V_{R2}=IR_{T2}$, and third and fourth ones, $V_{R3}=IR_{T3}$) and across a standard resistance, $V_I=IR_s$, were amplified and then were sent via an analog-digital (A/D) converter to a digital computer. The unbalance voltage, V_T, is expressed by means of Ohm's low as the following form.

$$V_T = \frac{I\left(R_T \times R_2 - R_1 \times R_3\right)}{R_2 + R_3} \tag{6}$$

These voltages were simultaneously sampled at a constant interval ranging from 60 to 200 ms. The average temperatures of the SUS304 test tube between the first and forth potential taps and between adjacent potential taps (first and second potential taps, second and third ones, and third and fourth ones) were calculated with the aid of previously calibrated resistance-temperature relation, $R_T=a(1+b\overline{T}+c\overline{T}^{\,2})$, respectively. The average temperatures of the test tube between the two electrodes, V_{R4}, were compared with those between first and fourth potential taps, V_R, and much difference for a heat loss could not be clearly observed in high subcooling range. The heat generation rates of the SUS304 test tube between the first and forth potential taps, $Q=I^2R_T$, and between adjacent potential taps (first and second potential taps, $Q_1=I^2R_{T1}$, second and third ones, $Q_2=I^2R_{T2}$, and third and fourth ones, $Q_3=I^2R_{T3}$) were calculated from the measured voltage difference between the first and forth potential taps and between adjacent potential taps of the SUS304 test tube, V_R, V_{R1}, V_{R2} and V_{R3}, and that across the standard resistance, V_I. The surface heat fluxes between the first and forth potential taps and between adjacent potential taps, q, q_1, q_2 and q_3, were the differences between the heat generation rate per unit surface area, Q, Q_1, Q_2 and Q_3, and the rate of change of energy storage in the SUS304 test tube obtained from the faired average temperature versus time curve as follows:

$$q = \frac{V}{S}\left(Q - \rho c \frac{d\overline{T}}{dt}\right) \tag{7}$$

where ρ, c, V and S were the density, the specific heat, the volume and the inner surface area of the SUS304 test tube, respectively.

The heater inner surface temperatures between the first and forth potential taps and between adjacent potential taps, T_s, T_{s1}, T_{s2} and T_{s3}, were also obtained by solving the steady one-dimensional heat conduction equation in the test tube under the conditions of measured average temperature, $\overline{T}$, and surface heat flux of the test tube, q. The solutions for the inner and outer surface temperatures of the test tube, T_s and T_{so}, were given by the steady one-dimensional heat conduction equation. The basic equation for the test tube is as follows:

$$\frac{d^2T}{dr^2}+\frac{1}{r}\frac{dT}{dr}+\frac{Q}{\lambda}=0 \tag{8}$$

then integration yields and the mean temperature of the test tube is obtained.

$$T(r)=-\frac{Qr^2}{4\lambda}+\frac{Qr_o^2}{2\lambda}\ln r+C \tag{9}$$

$$\overline{T}=\frac{1}{\pi\left(r_o^2-r_i^2\right)}\int_{r_i}^{r_o}2\pi rT(r)dr \tag{10}$$

Generating heat in the tube is equal to the heat conduction and the test tube is perfectly insulated.

$$q=-\lambda\left.\frac{dT}{dr}\right|_{r=r_i}=\frac{\left(r_o^2-r_i^2\right)Q}{2r_i} \tag{11}$$

$$\left.\frac{dT}{dr}\right|_{r=r_o}=0 \tag{12}$$

The temperatures of the heater inner and outer surfaces, T_s and T_{so}, and C in Eq. (9) can be described as follows:

$$T_s=T(r_i)=\overline{T}-\frac{qr_i}{4(r_o^2-r_i^2)^2\lambda}\left[4r_o^2\left\{r_o^2\left(\ln r_o-\frac{1}{2}\right)-r_i^2\left(\ln r_i-\frac{1}{2}\right)\right\}-\left(r_o^4-r_i^4\right)\right]-\frac{qr_i}{2(r_o^2-r_i^2)\lambda}\left(r_i^2-2r_o^2\ln r_i\right) \tag{13}$$

$$T_{so}=T(r_o)=\overline{T}-\frac{qr_i}{4(r_o^2-r_i^2)^2\lambda}\left[4r_o^2\left\{r_o^2\left(\ln r_o-\frac{1}{2}\right)-r_i^2\left(\ln r_i-\frac{1}{2}\right)\right\}-\left(r_o^4-r_i^4\right)\right]-\frac{qr_ir_o^2}{2(r_o^2-r_i^2)\lambda}\left(1-2\ln r_o\right) \tag{14}$$

$$C = \overline{T} - \frac{q r_i}{4(r_o^2 - r_i^2)^2 \lambda}\left[4r_o^2\left\{r_o^2\left(ln\, r_o - \frac{1}{2}\right) - r_i^2\left(ln\, r_i - \frac{1}{2}\right)\right\} - \left(r_o^4 - r_i^4\right)\right] \tag{15}$$

where $\overline{T}$, q, λ, r_i and r_o are average temperature of the test tube, heat flux, thermal conductivity, test tube inner radius and test tube outer radius, respectively.

In case of the 6-mm inner diameter test sections, before entering the test tube, the test water flows through the tube with the same inner diameter of the SUS304 test tube to form the fully developed velocity profile. The entrance tube lengths, L_e, are given 333 mm (L_e/d=55.5). The values of L_e/d for d=6 mm in which the center line velocity reaches 99 % of the maximum value for turbulence flow were obtained ranging from 9.8 to 21.9 ($1.50\times10^4 \le Re_d \le 1.575\times10^5$) by the correlation of Brodkey and Hershey [18] as follows:

$$\frac{L_e}{d} = 0.693 Re_d^{1/4} \tag{16}$$

The inlet and outlet liquid temperatures, T_{in} and T_{out}, were measured by 1-mm o.d., sheathed, K-type thermocouples (*Nimblox*, sheath material: SUS316, hot junction: ground, response time (63.2 %): 46.5 ms) which were located at the centerline of the tube at the upper and lower stream points of 283 and 63 mm from the tube inlet and outlet points for the 6-mm inner diameter test section. The inlet and outlet pressures, P_{ipt} and P_{opt}, were measured by the strain gauge transducers (Kyowa Electronic Instruments Co., Ltd., PHS-20A, Natural frequency: approximately 30 kHz), which were located near the entrance of conduit at upper and lower stream points of 63 mm from the tube inlet and outlet points for d=6 mm inner diameter test section. The thermocouples and the transducers were installed in the conduits as shown in Fig. 2.

The inlet and outlet pressures, P_{in} and P_{out}, for the 6-mm inner diameter test section were calculated from the pressures measured by inlet and outlet pressure transducers, P_{ipt} and P_{opt}, as follows:

$$P_{in} = P_{ipt} - \{(P_{ipt})_{wnh} - (P_{opt})_{wnh}\} \times \frac{L_{ipt}}{L_{ipt} + L + L_{opt}} \tag{17}$$

$$P_{out} = P_{in} - (P_{in} - P_{opt}) \times \frac{L}{L + L_{opt}} \tag{18}$$

where L_{ipt}=0.063 m and L_{opt}=0.063 m for the 6-mm inner diameter one. Experimental errors are estimated to be ±1 K in inner tube surface temperature and ±2 % in heat flux. Mass velocity, inlet and outlet subcoolings, inlet and outlet pressures and exponential period were measured within the accuracy ±2 %, ±1 K, ±4 kPa and ±2 %, respectively.

3. EXPERIMENTAL RESULTS AND DISCUSSION

3.1. Experimental Conditions

Steady-state heat transfer processes on the SUS304 circular test tube of 6 mm inner diameter that caused by the exponentially increasing heat inputs, $Q_0exp(t/\tau)$, were measured. The exponential periods, τ, of the heat input ranged from 7.02 to 8.51 s. The initial experimental conditions such as inlet flow velocity, inlet liquid temperature, inlet pressure and exponential period for the CHF experiment were determined independently each other before each experimental run.

The experimental conditions were as follows:

Test Tube Number	THD-F191 and THD-F196
Heater material	SUS304
Surface condition	Commercial finish of inner surface
Surface roughness	3.89 μm for *Ra*, 21.42 μm for *Rmax* and 15.03 μm for *Rz*
Inner diameter (d)	6 mm
Heated length (L)	59.5 and 59.7 mm

Effective Length (L_{eff})	49.0 and 50.2 mm
L_{12}, L_{23} and L_{34}	16.5, 16.8 and 15.7 mm for THD-F191 and
	16.8, 17.3 and 16.1 mm for THD-F196
L/d	9.92 and 9.95
L_{eff}/d	8.17 and 8.37
Wall thickness (δ)	0.5 mm
Inlet flow velocity (u)	3.95 to 30.80 m/s
Liquid Reynolds numbers (Re_d)	3.65×10^4 to 3.08×10^5
Inlet pressure (P_{in})	785.01 to 966.89 kPa
Outlet pressure (P_{out})	799.60 to 845.11 kPa
Inlet subcooling ($\Delta T_{sub,in}$)	141.35 to 159.03 K
Outlet subcooling ($\Delta T_{sub,out}$)	109.56 to 134.41 K
Inlet liquid temperature (T_{in})	288.10 to 308.73 K
Exponentially increasing heat input (Q)	$Q_0 exp(t/\tau)$, τ=7.02 to 8.51 s

3.2. Steady-state Heat Transfer Characteristics

3.2.1. SUS304 test tube of 6 mm inner diameter

Figure 5 shows the typical time variations in the inlet and outlet pressures calculated by Eqs. (17) and (18), P_{in} and P_{out}, heat flux, q, and heater inner and outer surface temperatures, T_s and T_{so}, inlet liquid temperature, T_{in}, outlet liquid temperature, T_{out}, flow velocity, u, and sound level meter signal, SLM, with time for P_{out}=831.8 kPa, $\Delta T_{sub,in}$=150.9 K and u=10.0 m/s. The test tube was heated with an exponentially increasing heat input with the period of 8.25 s. The heat flux becomes exponentially higher with an increase in the heat input per unit volume and reaches a maximum value, $q_{cr,sub}$, which is named the CHF.

The inner surface temperatures are almost constant at first and increase with an increase in the heat input, and those increase rate become lower for the boiling initiation. Those continue to increase up to the CHF and rapidly increase at the point. The values of the lower limit of the heterogeneous spontaneous nucleation temperature, T_{HET}, [19] and the homogeneous spontaneous nucleation temperature, T_H, [20] at the pressure of 800 kPa are shown in the figure as the red arrows for comparison. The inner surface temperatures of the test tube at CHF with the flow velocity, u, of 10.0 m/s are 32.07 K higher and 22.65 K lower than the T_{HET} and the T_H, respectively. The outer surface temperature of the test tube also increases with an increase in the heat input and that at CHF becomes 282.97 K higher than the inner surface temperature. These phenomena are also shown as plots of *log q* versus *log* ΔT_{sat} ($=T_s-T_{sat}$) and $\Delta T_{so,sat}$ ($=T_{so}-T_{sat}$) in Fig. 7 mentioned later. The values of P_{in} and P_{out} keep almost constant in the whole experimental range, and they are not observed to oscillate violently near the CHF point so that they did in the flow boiling heat transfer and CHF experiments for the platinum test tube of d=3 mm and L=66.5 mm [12]. The boiling initiation noise signal, BI, was finally measured from the elapsed time of 53.64 s by the sound level meter, SLM, although the real and faint sound wave for incipient boiling point would be drown out from the circulation noise of the canned type circulation pump. The sound wave captured by the microphone of the video camera, MP, with a picture was analyzed with applying wavelet methods (Wavelet Toolbox, The MathWorks, Inc.) and FFT (Fast Fourier Transform) ones. The typical time domains in the MP signals and the contour of various wavelet coefficients are plotted with time in Fig. 6. The boiling initiation point signal and the CHF point one are almost regarded in the same light as those for SLM as shown in Fig.5. The real and faint incipient boiling sound wave could not be made clear for circulation pump noise in this work.

Figure 7 shows typical examples of the heat transfer curves for the exponential period, τ, of around 8.11 s on the SUS304 test tube (THD-F191) of d=6 mm and L=59.5 mm with the rough finished inner surface (Ra=3.89 μm) at the inlet liquid temperature, T_{in}, of 288.10 to 309.54 K and the flow velocities, u, of 3.95

to 30.80 m/s. At the flow velocities of 4.0, 6.9, 9.9 and 13.3 m/s (red, pink, green and sky-blue solid lines), the heat flux gradually becomes higher with an increase in inner surface superheat, ΔT_{sat} ($=T_s$-T_{sat}, T_s: heater inner surface temperature and T_{sat}: saturation temperature), on the non-boiling forced convection curve derived from our correlation, Eq. (1), [1, 2] up to the point where the slope begins to increase with heat flux following the onset of nucleate boiling. After that the heat flux increases along the fully developed nucleate boiling curve on the graph up to the CHF, at which the transition to film boiling occurs with the rapidly increasing of surface superheat. It is assumed that the transition to film boiling would occur due to the liquid sub-layer dry-out model [17] suggested by Lee and Mudawar [21], Katto [22] and Celata et. al. [23] but not due to the hydro-dynamic instability suggested by Kutateladze [24] and Zuber [25]. At flow velocities of 17, 21 and 30 m/s (grey, blue and black solid lines), the heat flux gradually becomes higher with an increase in ΔT_{sat} on the non-boiling forced convection curve derived from our correlation, Eq. (1), up to the CHF, at which the transition to film boiling occurs on the non-boiling forced convection curve. Although the violent boiling noise was made for a period of time before the CHF point, the slope on the boiling curve does not increase with heat flux even following the onset of nucleate boiling. It is assumed that the semi-direct transition from non-boiling regime to film boiling with nucleate boiling would occur due to the heterogeneous spontaneous nucleation at the lower limit of the heterogeneous spontaneous nucleation temperature even at the steady-state CHF [26] but not due to the hydro-dynamic instability and the liquid sub-layer dry-out models. However the CHFs do not extremely become lower than the values calculated from our CHF correlations, Eqs. (3) and (5). The CHF and its surface superheat become higher with an increase in flow velocity. The values of CHF numerically analyzed from Celata et. al.'s liquid sub-layer dry-out model [23] are shown in Fig. 7 as the arrows with each color for comparison. The values derived from liquid sub-layer dry-out model are in good agreement with the experimental values of CHF for the SUS304 test tube of d=6 mm and L=59.5 mm within -10.66, 4.44, 0.074, -0.901 and 5.98 % differences at the flow velocities of 7.04, 9.97, 13.40, 17.17 and 21.22 m/s, respectively, as shown in Table1. However, at flow velocities of 17 and 21 m/s (grey and blue solid lines), the slopes on the boiling curves do not increase with heat flux even following the onset of nucleate boiling as shown in Fig. 7 and the transitions to film boiling occur on the non-boiling forced convection curves with high surface superheats, ΔT_{sat}, over to the homogeneous spontaneous nucleation temperature as well as the lower limit of the heterogeneous spontaneous nucleation temperature as mentioned later, although the experimental values of CHFs are in good agreement with the values derived from liquid sub-layer dry-out model. It is assumed from these facts that the thicknesses of conductive sub-layer would exist not to dissipate by the evaporation on nucleate boiling and the transition to film boiling due to the heterogeneous spontaneous nucleation at the lower limit of the heterogeneous spontaneous nucleation temperature would be the dominant mechanism of these CHFs. The test loop needs first to be validated with the single-phase tests confirming other researchers' correlations. These comparisons are shown in Appendix A.1. Many researchers gave CHF models and correlations of subcooled flow boiling. These comparisons are shown in Appendix A.2.

The boiling initiation noise surface heat fluxes and surface superheats at the BI points, (q_{BI}, ΔT_{BI}), which were judged by SLM and the wavelet coefficient in Fig. 7 are indicated with open circles with symbol colors in the figure. It is like the signals that these are late from the real and faint incipient boiling sound wave because these heat fluxes at BI points are a little higher than the turbulent heat transfer coefficients calculated from Eq. (1). The fully developed nucleate boiling curves for the flow velocity lower than 13.3 m/s and the heat transfer curves in higher heat flux range for the flow velocity higher than 17 m/s agree with each other forming a single straight line calculated from Eq. (19) on the *log q* versus *log* ΔT_{sat} graph.

$$q = C\Delta T_{sat}^{n} = 1.065\times10^{5}\Delta T_{sat}^{1.2} \tag{19}$$

where C and n are coefficient and exponent, and equivalent to 1.065×10^{5} and 1.2 respectively. The correlation can almost describe the fully developed nucleate boiling curves for the flow velocity lower than 13.3 m/s and the nucleate boiling curves in higher heat flux range for the flow velocity higher than 17 m/s, which were obtained on the SUS304 test tubes (THD-F191 and F196) of d=6 mm and L=59.5 mm with the rough finished inner surface at the outlet pressure of around 800 kPa in this work, within ±30 % differences under the wide range of flow velocities.

The analytical solution of incipient boiling superheat given by Sato and Matsumura [27] is shown in Fig. 7 for comparison. The solution was derived based on the initiation model of bubble growth.

$$q = \frac{\lambda_l h_{fg} \left(T_s - T_{sat}\right)^2}{8\sigma T_{sat} \left(v_g - v_l\right)} \tag{20}$$

For thermo-physical properties, the saturated temperature, T_{sat}, is defined. The experimental data of the incipient boiling superheat almost agree with the values predicted by Eq. (20) for the flow velocities of 4 and 6.9 m/s, although those for the flow velocities of 9.9 and 13.3 m/s are slightly lower than those predicted by Eq. (20). The equation of incipient boiling superheat given by Bergles and Rohsenow [28] is also shown in the figure for comparison.

$$(\Delta T_{sat})_{ONB} = 0.556\left(\frac{q}{1082P^{1.156}}\right)^{0.463P^{0.0234}} \tag{21}$$

where q is the surface heat flux in W/m^2, P is the system pressure in bar and ΔT_{sat} is in K. The corresponding curves derived from the correlations for fully developed subcooled boiling given by Rohsenow [29] are also shown in Fig. 7 for comparison.

$$\frac{c_{pl}\Delta T_{sat}}{h_{fg}} = C_{sf}\left(\frac{q}{\mu_l h_{fg}}\sqrt{\frac{\sigma}{g(\rho_l - \rho_g)}}\right)^{0.33}\left(\frac{c_{pl}\mu_l}{\lambda_l}\right)^{1.7} \tag{22}$$

where the various fluid properties are evaluated at the saturation temperature corresponding to the local pressure and C_{sf} is a function of the particular heating surface-fluid combination. The value of n given by Rohsenow correlation, Eq. (22), with C_{sf}=0.03 is about 2.5 times larger than that of our correlation, Eq. (19), on the *log q* versus *log* ΔT_{sat} graph.

The values of the lower limit of the heterogeneous spontaneous nucleation temperature, T_{HET}, [19] and the homogeneous spontaneous nucleation temperature, T_H, [20] at the pressure of 800 kPa are shown in the figure for comparison. The inner surface temperature of the test tube at CHF with the flow velocity, u, of 30 m/s is almost 143.13 and 88.41 K higher than the lower limit of the heterogeneous spontaneous nucleation temperature and the homogeneous spontaneous nucleation temperature, respectively.

Figure 7 also shows the relation between the heat flux, q, and the outer surface temperature of the test tube in the open air, T_{so}, on the $log\ q$ versus $log\ \Delta T_{so,sat}$ ($=T_{so}-T_{sat}$) graph for the SUS304 test tube (THD-F191) of d=6 mm and L=59.5 mm with the rough finished inner surface (Ra=3.89 μm) with the exponential period of 8.11 s at the flow velocities of 4.0, 6.9, 9.9, 13.3, 17, 21 and 30 m/s (red, pink, green, sky-blue, grey, blue and black one dot broken lines). The values of T_{so} are derived from our correlation, Eq. (14). And the outer surface temperatures of the test tube, T_{so}, were continuously measured in the time interval of 3 seconds by an infrared thermal imaging camera (ITIC). These experimental data for the flow velocities of 4.0, 9.9, 21 and 30 m/s are shown as solid circles with each symbol color in the figure. These outer surface temperatures were almost 8 % lower than the values calculated from Eq. (14) for each heat flux in the whole velocity, although the infrared thermal imaging camera has the accuracy of ±2 % of reading. The color temperatures of outer surface of the test tube in the open air have been observed by a video camera (VC) and the typical photographs at each CHF point are shown in Fig. 8 for flow velocities of 4, 9.9, 21 and 30 m/s. The color temperature of outer surface of the test tube at the flow velocity of 30 m/s would reach up to around 1173 K because the test tube begins to be shining white. The outer surface temperature becomes very high at the CHF. It is assumed from these facts that the CHFs on the SUS304 test tube would explicitly occur due to the heterogeneous spontaneous nucleation with combinations of non-boiling forced convection heat transfer and heterogeneous spontaneous nucleation temperature in independence of surface conditions such as surface roughness and surface wettability for the flow velocity higher than 17 m/s [26]. Cavities of submicron sizes from which bubble nucleation can occur at high surface superheat and heat flux would exist but not sufficient in their numbers to flatten the temperature gradient near the heated surface through the bubble motion and the latent heat transport.

Therefore, the nucleate boiling heat transfer for higher flow velocity would be like the non-boiling forced convection one. Considering that the outer surface of the test tube is glowing at 1173 K, the radiation heat loss would be significant. Mention of radiative and convective losses is made in Appendix A.3.

Under the vertical test tubes in this work, the effects of the flow velocity on boiling initiation noise surface superheat, ΔT_{BI}, heater inner surface superheat, ΔT_{sat} (=T_s-T_{sat}), at the CHF point, $(\Delta T_{sat})_{cr}$ and heater outer surface superheat, $\Delta T_{so,sat}$ (=T_{so}-T_{sat}), at the CHF point, $(\Delta T_{so,sat})_{cr}$, for the vertical SUS304 tube of d=6 mm was represented versus the flow velocity, u, in Fig. 9. The values of ΔT_{BI} (△, △ and △), $(\Delta T_{sat})_{cr}$ (■, ■ and ■) and $(\Delta T_{so,sat})_{cr}$ (□, □ and □) for vertical SUS304 test tube of d=6 mm in this work become linearly higher with an increase in the flow velocity for the flow velocities ranging from 3.95 to 30.80 m/s, respectively. These values can be expressed by the following correlations:

$$\Delta T_{BI} = 6.87u^{0.96} \qquad \text{for } \Delta T_{BI} \qquad (23)$$

$$(\Delta T_{sat})_{cr} = 27.63u^{0.6} \qquad \text{for } (\Delta T_{sat})_{cr} \qquad (24)$$

$$(\Delta T_{so,sat})_{cr} = 125u^{0.5} \qquad \text{for } (\Delta T_{so,sat})_{cr} \qquad (25)$$

It is contemplated especially in case of this vertical SUS304 test tube that the values of $(\Delta T_{sat})_{cr}$, (■, ■ and ■), would become linearly higher with an increase in the flow velocity from around the lower limit of heterogeneous spontaneous nucleation temperature due to a combination between surface conditions of test tubes. The discrepancy between surface conditions such as surface roughness and surface wettability would play an important role in nucleate boiling heat transfer at the CHF points. The values of $(\Delta T_{so,sat})_{cr}$, (□, □ and □), for vertical SUS304 test tube of d=6 mm in this work also become linearly higher with an increase in the flow velocity for the flow velocities ranging from 3.95 to 30.80 m/s. These values of $(\Delta T_{sat})_{cr}$ and $(\Delta T_{so,sat})_{cr}$, (■ and □) for SUS304 test tube (THD-F196) become T_s=494.27 and T_{so}=712.44 K at u=4 m/s, T_s=556.11 and T_{so}=839.08 K at u=9.9 m/s, T_s=591.97 and T_{so}=980.38 K at u=21 m/s and T_s=667.20 and T_{so}=1170.93 K at u=30 m/s, respectively. The effects of flow velocity on the values of boiling initiation noise surface heat flux and steady-state critical heat flux, q_{BI} and $q_{cr,sub,st}$, for the vertical

SUS304 tubes of d=6 mm were represented versus the flow velocity, u, in Fig. 10. The values of the q_{BI} can be expressed by the following correlation and those of the $q_{cr,sub,st}$ can be done by Eq. (4) for the flow velocity lower than 13.3 m/s and by Eq. (5) for the flow velocity higher than 13.3 m/s:

$$q_{BI} = 1.2 \times 10^6 u^{1.07} \qquad \text{for } q_{BI} \tag{26}$$

It is assumed from these facts as shown in Figs 9 and 10 that the margins up to the CHF points would not be in enough existence at the boiling initiation noise points for the flow velocities higher than 13.3 m/s.

Figure 11 shows the steady-state CHFs, $q_{cr,sub,st}$, versus the outlet subcoolings, $\Delta T_{sub,out}$, for the vertical SUS304 circular test tube of the inner diameter (d=6 mm), the heated length (L=59.5 mm), L/d (=9.92) and the wall thickness (δ=0.5 mm) obtained for the flow velocities, u, ranging from 3.95 to 30.8 m/s at the outlet pressure, P_{out}, of around 800 kPa. The CHF data for the vertical SUS304 test tubes of d=6 mm, L=59.5 and 66 mm, L/d =9.92 and 11 and δ=0.5 mm with the flow velocities ranging from 4.0 to 40 m/s are also shown in the figure for comparison [3, 11, 14]. As shown in the figure, the $q_{cr,sub,st}$ for each flow velocity become higher with an increase in $\Delta T_{sub,out}$ and the increasing rate becomes lower for higher $\Delta T_{sub,out}$. The CHFs in the whole experimental range become higher with an increase in the flow velocity at a fixed $\Delta T_{sub,out}$. The curves given by Eqs. (2) and (3) for the vertical SUS304 circular test tube are shown in Fig. 11 at each flow velocity for comparison. The CHF data for $\Delta T_{sub,out}\geq$30 K are in good agreement with the values given by the correlations. Equations (2) and (3) were derived based on the experimental data for the vertical SUS304 test tube with the flow velocities ranging from 4 to 13.3 m/s and ranging from 17 to 40 m/s respectively. To confirm the applicability of Eqs. (2) and (3) to the data for the flow velocity of 4 to 40 m/s, the ratios of these CHF data to the corresponding values calculated by Eqs. (2) and (3) are shown versus $\Delta T_{sub,out}$ in Fig. 12. Most of the data for the vertical circular test tube (266 points) [3, 11, 14] and the current data (47 points) are within ±15 % differences for 3.95 m/s$\leq u \leq$40 m/s and 109.56 K$\leq \Delta T_{sub,out} \leq$134.41 K. It can be considered that the CHFs are determined not by the outlet conditions but by the inlet ones. The steady-state CHFs, $q_{cr,sub,st}$, for the vertical SUS304 circular test tube of the inner diameter of 6 mm, L=59.5 mm, L/d=9.92 and δ=0.5 mm were shown versus the inlet subcooling, $\Delta T_{sub,in}$, with the flow velocities of 4 to 13.3 m/s in Fig. 13. The CHF data for the vertical SUS304 test tube of d=6 mm, L=59.5 and 66 mm, L/d =9.92 and 11 and δ=0.5 mm with the flow velocities ranging from 4.0 to 40 m/s are also shown in the figure for comparison [3, 11, 14]. The $q_{cr,sub,st}$ for each flow velocity become higher with an increase in $\Delta T_{sub,in}$. The increasing rate becomes also lower for higher $\Delta T_{sub,in}$. The $q_{cr,sub,st}$ increase with an increase in the flow velocity at a fixed $\Delta T_{sub,in}$. The $q_{cr,sub,st}$ for the wide range of flow velocities are proportional to $\Delta T_{sub,in}^{0.7}$ for $\Delta T_{sub,in}$≥40 K. The curves derived from Eqs. (4) and (5) for the vertical SUS304 circular test tube are shown in Fig. 13 for comparison. The CHF data for $\Delta T_{sub,in}$≥40 K are in good agreement with the values given by authors' correlation. To confirm the applicability of Eqs. (4) and (5), the ratios of these CHF data for the d=6 mm vertical circular test tube (266 points) [3, 11, 14] and those for the d=6 mm current one (47 points) to the corresponding values calculated by Eqs. (4) and (5) are shown versus $\Delta T_{sub,in}$ in Fig. 14. Most of the data for $\Delta T_{sub,in}$≥40 K are within ±15 % differences of Eqs. (4) and (5) for 3.95 m/s≤u≤40 m/s and 141.35 K≤$\Delta T_{sub,in}$≤159.03 K.

To confirm the margins up to the CHF points at the boiling initiation noise points for the flow velocity of 4 to 30.8 m/s, the ratios of the BI surface heat flux data to the CHF data and the values derived from the outlet CHF correlations and those of the BI surface heat flux data to the CHF data and the values derived from the inlet CHF correlations are shown versus u for outlet subcooling, $\Delta T_{sub,out}$, and inlet subcooling, $\Delta T_{sub,in}$, in Figs. 15 and 16, respectively. These ratios of q_{BI} to $q_{cr,sub,st}$ for the vertical SUS304 circular test tube of the inner diameter of 6 mm were made a comparison between the following correlation:

$$\frac{q_{BI}}{q_{cr,sub,st}} = 0.181 u^{0.5} \qquad \text{for ratio of } q_{BI} \text{ to } q_{cr,sub,st} \qquad (27)$$

It was able to be also confirmed from these figures that the margins up to the CHF points at the boiling initiation noise points would not be in enough existence for the flow velocity higher than 13.3 m/s in the same way as Figs 9 and 10.

4. CONCLUSIONS

The subcooled boiling heat transfer and the steady-state critical heat flux (CHF) in a vertical circular tube for the liquid Reynolds numbers (Re_d=3.65×10^4 to 3.08×10^5), the flow velocities (u=3.95 to 30.80 m/s) were systematically measured. The SUS304 test tube of inner diameter (d=6 mm) and heated length (L=59.5 mm) was used in this work. The boiling initiation noise of outer surface of the test tube in the open air was simultaneously measured up to CHF point by the sound level meter (SLM) and the microphone of a video camera (MP). The outer surface temperatures of the SUS304 test tube with heating were also observed by an infrared thermal imaging camera (ITIC) and the color temperatures of outer surface of the test tube in the open air were observed by a video camera (VC). Experimental study results lead to the following conclusions.

1) At the flow velocities of 4.0, 6.9, 9.9 and 13.3 m/s, the transition to film boiling would occur due to the liquid sub-layer dry-out model.
2) At the flow velocities of 17, 21 and 30 m/s, the semi-direct transition from non-boiling regime to film boiling with nucleate boiling would occur due to the heterogeneous spontaneous nucleation at the lower limit of the heterogeneous spontaneous nucleation temperature even at the steady-state CHF.
3) The boiling initiation noise surface superheat, ΔT_{BI}, heater inner surface superheat at the CHF point, $(\Delta T_{sat})_{cr}$, and heater outer surface superheat at the CHF point, $(\Delta T_{so,sat})_{cr}$, for the vertical SUS304 tube of d=6 mm can be expressed by Eqs. (23) to (25).

4) Most of the steady-state CHF data for SUS304 circular tube of d=6 mm at high liquid Reynolds number with 3.95 m/s≤u≤30.8 m/s (47 points) are within ±15 % differences of Eqs. (2) and (3) for 109.56 K≤$\Delta T_{sub,out}$≤134.41 K and within ±15 % differences of Eqs. (4) and (5) for 3.95 m/s≤u≤30.8 m/s and 141.35 K≤$\Delta T_{sub,in}$≤159.03 K.

5) The ratios of the BI surface heat flux data for the vertical SUS304 circular test tube of d=6 mm to the CHF data and the values derived from the outlet and inlet CHF correlations, $q_{BI}/q_{cr,sub,st}$, were made a comparison between Eq. (27). The margins up to the CHF points at the boiling initiation noise points would not be in enough existence for the flow velocity higher than 13.3 m/s.

NOMENCLATURE

Bo $=q/Gh_{fg}$, boiling number

Bo_{cr} $=q_{cr,sub,st}/Gh_{fg}$, boiling number at CHF point

C_1, C_2, C_3, C_4, C_5, C_6 constants in Eqs. (4) and (5)

c specific heat, J/kgK

c_{pl} specific heat at constant pressure, J/kgK

d test tube inner diameter, m

d_o test tube outer diameter, m

E_b energy radiated per unit time and per unit area, W/m^2

G $=\rho_l u$, mass velocity, kg/m^{2}s

g acceleration of gravity, m/s^2

h_{fg} latent heat of vaporization, J/kg

L heated length, m

L_{eff} effective length, m

Nu_d $=hd/\lambda_l$, nusselt number

P_{cr} =22064 kPa, critical pressure, kPa

P_{in} pressure at inlet of heated section, kPa

P_{ipt} pressure measured by inlet pressure transducer, kPa

P_{out} pressure at outlet of heated section, kPa

P_{opt} pressure measured by outlet pressure transducer, kPa

Pr $=c_p\mu/\lambda$, Prandtl number

P_r $=P_{out}/P_{cr}$, reduced pressure, kPa

Q heat input per unit volume, W/m^3

Q_0 initial exponential heat input, W/m^3

$Q_{cr,sub,st}$ total heat, W

q heat flux, W/m^2

$q_{cr,sub,st}$ steady-state CHF for subcooled condition, W/m^2

q_r radiative heat flux, W/m^2

Ra average roughness, μm

Re_d $=Gd/\mu_l$, Reynolds number

$Rmax$ maximum roughness depth, μm

Rz mean roughness depth, μm

r_i test tube inner radius, m

r_o test tube outer radius, m

Sc $=c_{pl}\Delta T_{sub,out}/h_{fg}$, non-dimensional outlet subcooling

$Sc*$ $=c_{pl}\Delta T_{sub,in}/h_{fg}$, non-dimensional inlet subcooling

T temperature of the test tube, K

$\overline{T}$ average temperature of test tube, K

T_b room temperature, K

$T_{f,av}$ average liquid temperature, K

T_{in} inlet liquid temperature, K

T_L $=(T_{in}+T_{out})/2$, liquid bulk mean temperature, K

T_{out} outlet liquid temperature, K

$(T_{out})_{cal}$ calculated outlet liquid temperature, K

T_s heater inner surface temperature, K

$T_{sat,in}$ saturation temperature at inlet of heated section, K

$T_{sat,out}$ saturation temperature at outlet of heated section, K

T_{sat} saturation temperature, K

T_{so} heater outer surface temperature, K

$T_{s,av}$ average inner surface temperature, K

ΔT_L $=(T_{s,av}-T_L)$, temperature difference between average inner surface temperature and liquid bulk mean temperature, K

ΔT_{sat} $=T_s-T_{sat}$, inner surface superheat, K

$\Delta T_{sat,so}$ $=T_s-T_{sat}$, outer surface superheat, K

u flow velocity, m/s

We $=G^2d/\rho_l\sigma$, Weber number

Y Shah correlating parameter

ε emissivity

λ thermal conductivity, W/mK

λ_l thermal conductivity, W/mK

μ_g viscosity, Ns/m^2

μ_l viscosity, Ns/m^2

μ_w viscosity at tube wall temperature, Ns/m^2

ρ density, kg/m^3

σ $=5.669\times10^{-8}$, Stefan-Boltzmann constant, W/m^{2}K^4

τ exponential period, s

χ vaper quality

χ_c vaper quality at location of CHF

		out	outlet
Subscript		*l*	liquid
cr	critical	*sat*	saturated condition
g	vapor	*sub*	subcooled condition
in	inlet	*wnh*	with no heating

ACKNOWLEDGMENTS

This research was performed as a LHD joint research project of NIFS (National Institute for Fusion Science), Japan, NIFS13KEMF054, 2014.

APPENDIX A

A.1. Single-phase Tests [1, 2]

Many researchers have experimentally studied the steady-state turbulent heat transfer in pipes and given the correlations for calculating steady-state turbulent heat transfer coefficients [30- 34].

- Dittus and Boelter [30]: $Nu_d = 0.023 Re_d^{0.8} Pr^{0.4}$ (28)
- Nusselt [31]: $Nu_d = 0.036 Re_d^{0.8} Pr^{1/3} \left(\frac{d}{L}\right)^{0.055}$ (29)
- Sieder and Tate [32]: $Nu_d = 0.027 Re_d^{0.8} Pr^{1/3} \left(\frac{\mu_l}{\mu_w}\right)^{0.14}$ (30)
- Petukhov [33]: $Nu_d = \frac{(f/2) Re_d Pr}{1.07 + 12.7 (f/2)^{1/2} (Pr^{2/3} - 1)}$ (31)
- Gnielinski [34]: $Nu_d = \frac{(f/2)(Re_d - 1000) Pr}{1 + 12.7 (f/2)^{1/2} (Pr^{2/3} - 1)}$ (32)

Figure 17 shows typical examples of the heat transfer curves for the exponential period, τ, of around 8.11 s on the SUS304 test tube (THD-F191) of d=6 mm and L=59.5 mm with the rough finished inner surface (Ra=3.89 μm) at the inlet liquid temperature, T_{in}, of 288.10 to 309.54 K and the flow velocities, u, of 3.95 to 30.80 m/s. At the flow velocities of 4.0, 13.3 and 30 m/s (red, sky-blue and black solid lines), the heat flux gradually becomes higher with an increase in inner surface superheat, ΔT_{sat} (=T_s-T_{sat}, T_s: heater inner surface temperature and T_{sat}: saturation temperature), on the non-boiling forced convection curve (black broken line) derived from our correlation, Eq. (1), [1, 2] up to the point where the slope begins to increase with heat flux following the onset of nucleate boiling. The experimental data are also compared with the values derived from other researchers' correlations, Dittus and Boelter, Nusselt, Sieder and Tate, Petukhov and Gnielinski ones, Eqs. (28), (29), (30), (31) and (32), in Fig. 17 (blue, grey, pink, red and green broken lines). The values of heat flux calculated from Eqs. (28), (29), (30), (31) and (32) are 35.4 to 41.3 % lower, 21.4 to 25.9 % lower, 14.9 to 22.5 % lower, 27.6 to 31.6 % lower and 29.4 to 30.3 % lower than the experimental data at ΔT_{sat}=1 K.

A.2. Comparison of the Measured CHFs with Author's Correlations, and Other Researchers' CHF Model and Correlations.

Celata et al. [23] presented a mechanistic model for prediction of CHF in flow boiling of subcooled water. Hall and Mudawar [35] developed the inlet and outlet condition correlations for subcooled high-CHF base on the experimental data. Hall and Mudawar correlation [35] for the outlet conditions is as follows:

$$Bo_{cr} = 0.0332 We^{-0.235}\left(\frac{\rho_l}{\rho_g}\right)^{-0.681}\left[1-0.6837\left(\frac{\rho_l}{\rho_g}\right)^{0.832}\chi_{out}\right] \qquad \text{for outlet} \qquad (33)$$

Shah [36, 37] presented the upstream-conditions correlation (UCC) and the local-conditions correlation (LCC) for CHF in vertical tubes. Shah correlation for the LCC version [37] is as follows:

$$Bo_{cr} = F_E F_x Bo_0 \qquad \text{for the LCC version} \qquad (34)$$

Parameter Bo_0 has the highest value provided by the following three expressions:

$$Bo_0 = 15 Y^{-0.612} \qquad (35)$$

$$Bo_0 = 0.082 Y^{-0.3}\left[1+1.45 Pr^{4.03}\right] \qquad (36)$$

$$Bo_0 = 0.0024 Y^{-0.105}\left[1+1.15 Pr^{3.39}\right] \qquad (37)$$

where P_r=P_{out}/P_{cr} is the reduced pressure and P_{cr} (=22064 kPa) is the critical pressure.

The Shah correlating parameter Y [37] is defined as

$$Y = \frac{Gdc_{pl}}{\lambda_l}\left(Fr^2\right)^{0.4}\left(\frac{\mu_l}{\mu_g}\right)^{0.6} \tag{38}$$

where $Fr=u/\sqrt{(gd)}$ is the Froude number.

If $\chi_c < 0$,

$$F_x = F_1\left[1-\frac{(1-F_2)(P_r-0.6)}{0.35}\right]^b \tag{39}$$

$$F_1 = 1+0.0052(-\chi_c)^{0.88}Y^{0.41} \tag{40}$$

If $Y \geq 1.4\times10^7$, then $Y=1.4\times10^7$ must be used in Eq. (40). Also

$$F_2=F_1^{-0.42} \text{ when } F_1 \leq 4 \tag{41}$$

$$F_2=0.55 \text{ when } F_1 > 4 \tag{42}$$

$$b=0 \text{ for } P_r \leq 0.6 \tag{43}$$

$$b=1 \text{ for } P_r > 0.6 \tag{44}$$

The experimental data for u=4 to 30 m/s at P_{out}=800 kPa are compare with authors' correlations, Eqs. (2) and (3), solutions of the model by Celata et al. [23], Hall and Mudawar correlation, Eq. (33), and Shah correlation for the LCC version, Eq. (34), in Fig. 18 and Table 2 for the THD-F191 SUS304 test tube of d=6 mm and L=59.5 mm with the rough finished inner surface. The authors' correlations, Eqs. (2) and (3), solutions of the model by Celata et al., Hall and Mudawar correlation, Eq. (33), and Shah correlation for the LCC version, Eq. (34), are in good agreement with the experimental data for u=4 to 30 m/s within -17.91 to 24.23 % differences, -22.83 to 25.36 % differences, -26.16 to 2.91 % differences and -27.70 to 0.93 % differences, respectively.

A.3. Radiative and Convective Losses

The energy radiated per unit time and per unit area by the ideal radiator is proportional to absolute temperature to fourth power:

$$E_b = \sigma T^4 \tag{45}$$

The radiative heat flux, q_r, arriving at some area in the closure is calculated from

$$q_r = \sigma \varepsilon_w \times 10^8 \left[\left(\frac{T_{so}}{100} \right)^4 - \left(\frac{T_b}{100} \right)^4 \right] \tag{46}$$

where σ, ε_w, T_{so} and T_b are the Stefan-Boltzmann constant (=5.669×10^{-8} W/m^{2}K^4), the total emissivity of body (=0.211 at 1173 K for SUS304), the heater outer surface temperature (=1173 K) and the room temperature (=303 K). The total heat lost by the outer surface of the test tube, Q_r, is

$$Q_r = q_r \times \pi d_o L = 5.669 \times 10^{-8} \times 0.211 \times 10^8 \left[\left(\frac{1173}{100} \right)^4 - \left(\frac{303}{100} \right)^4 \right] \times 3.14 \times 0.007 \times 0.0595 = 29.484 W \tag{47}$$

where d_o and L are the test tube outer diameter and the heated length. As shown in Fig.7, the total heat received by the test water from the inner surface of the test tube at CHF point with u=30 m/s, $Q_{cr,sub,st}$, is

$$Q_{cr,sub,st} = q_{cr,sub,st} \times \pi d L = 50 \times 10^6 \times 3.14 \times 0.006 \times 0.0595 = 560490\, W \tag{48}$$

The radiation heat loss rate would be therefore negligible small 0.0526 % in comparison with the total heat generation of the test tube at CHF point.

$$radiation heat loss\ rate = \frac{Q_r}{Q_{cr,sub,st} + Q_r} = \frac{29.484}{29.484 + 56049.0} \times 100 = 0.0526\% \tag{49}$$

REFERENCES

1. K. Hata and N. Noda, “Turbulent Heat Transfer for Heating of Water in a Short Vertical Tube,” *Journal of Power and Energy Systems*, **2**, No. 1, pp. 318-329 (2008).

2. K. Hata, Y. Shirai, S. Masuzaki, and A. Hamura, “Computational Study of Turbulent Heat Transfer for Heating of Water in a Short Vertical Tube under Velocities Controlled,” *Nuclear Engineering and Design*, **249**, pp. 304-317 (2012).

3. K. Hata, M. Shiotsu and N. Noda, "Critical Heat Fluxes of Subcooled Water Flow Boiling against

Outlet Subcooling in Short Vertical Tube," *Journal of Heat Transfer*, Trans. ASME, Series C, **126**, pp. 312-320 (2004).

4. K. Hata, H. Komori, M. Shiotsu and N. Noda, "Critical Heat Fluxes of Subcooled Water Flow Boiling against Inlet Subcooling in Short Vertical Tube," *JSME International Journal*, Series B, **47**, No. 2, pp. 306-315 (2004).
5. K. Hata and N. Noda, "Thermal Analysis on Flat-Plate Type Divertor Based on Subcooled Flow Boiling Critical Heat Flux Data against Inlet Subcooling in Short Vertical Tube," *Journal of Heat Transfer*, Trans. ASME, Series C, **128**, pp. 311-317 (2006).
6. K. Hata, M. Shiotsu and N. Noda, "Thermal Analysis on Mono-Block Type Divertor Based on Subcooled Flow Boiling Critical Heat Flux Data against Inlet Subcooling in Short Vertical Tube," *Plasma and Fusion Research*, **1**, No. 017, pp. 1-10 (2006).
7. K. Hata, M. Shiotsu and N. Noda, "Critical Heat Flux of Subcooled Water Flow Boiling for High *L/d* Region," *Nuclear Science and Engineering*, **154**, No. 1, pp. 94-109 (2006).
8. K. Hata, M. Shiotsu and N. Noda, "Influence of Heating Rate on Subcooled Flow Boiling Critical Heat Flux in a Short Vertical Tube," *JSME International Journal*, Series B, **49**, No. 2, pp. 309-317 (2006).
9. K. Hata, M. Shiotsu and N. Noda, "Influence of Test Tube Material on Subcooled Flow Boiling Critical Heat Flux in Short Vertical Tube," *Journal of Power and Energy Systems*, **1**, No. 1, pp. 49-63 (2007).
10. K. Hata and N. Noda, "Transient Critical Heat Fluxes of Subcooled Water Flow Boiling in a Short Vertical Tube Caused by Exponentially Increasing Heat Inputs," *Journal of Heat Transfer*, Trans. ASME, Series C, **130**, pp. 054503-1-9 (2008).
11. K. Hata and S. Masuzaki, "Subcooled Boiling Heat Transfer in a Short Vertical SUS304-Tube at Liquid Reynolds Number Range 5.19×10^4 to 7.43×10^5," *Nuclear Engineering and Design*, **239**, pp. 2885-2907 (2009).
12. K. Hata and S. Masuzaki, "Subcooled Boiling Heat Transfer for Turbulent Flow of Water in a Short Vertical Tube," *Journal of Heat Transfer*, Trans. ASME, Series C, **132**, pp. 011501-1-11 (2010).

13. K. Hata and S. Masuzaki, "Influence of Heat Input Waveform on Transient Critical Heat Flux of Subcooled Water Flow Boiling in a Short Vertical Tube," *Nuclear Engineering and Design*, **240**, pp. 440-452 (2010).

14. K. Hata and S. Masuzaki, "Critical Heat Fluxes of Subcooled Water Flow Boiling in a Short Vertical Tube at High Liquid Reynolds Number," *Nuclear Engineering and Design*, **240**, pp. 3145-3157 (2010).

15. K. Hata, Y. Shirai and S. Masuzaki, "Heat Transfer and Critical Heat Flux of Subcooled Water Flow Boiling in a Horizontal Circular Tube," *Experimental Thermal and Fluid Science*, **44**, pp. 844-857 (2013).

16. K. Hata, K. Fukuda and S. Masuzaki, "Transient Critical Heat Fluxes of Subcooled Water Flow Boiling in a SUS304-Circular Tube caused by a Rapid Decrease in Velocity from Non-Boiling Regime," *Experimental Thermal and Fluid Science*, **66**, pp. 160-172 (2015).

17. K. Hata, K. Fukuda and S. Masuzaki, "Mechanism of Critical Heat Flux during Flow Boiling of Subcooled Water in a Circular Tube at High Liquid Reynolds Number," *Experimental Thermal and Fluid Science*, http://dx.doi.org/10.1016/j.expthermflusci.2015.09.015, **70**, pp. 255-269 (2016).

18. R. S. Brodkey and H. C. Hershey, "Transport Phenomena, McGraw-Hill," New York, p. 568 (1988).

19. C. Cole, "Homogeneous and heterogeneous nucleation in Boiling Phenomena," Vol. 1, Stralen, S. van, and Cole, R. eds., Hemisphere Pub. Corp., New York, p. 71 (1979).

20. J. H. Lienhard, "Correlation of Limiting Liquid Superheat," *Chem. Eng. Science*, **31**, pp. 847-849 (1976).

21. C. H. Lee, and I. Mudawar, "A mechanistic critical heat flux model for subcooled flow boiling based on local bulk flow conditions," *International Journal of Multiphase Flow*, **14**, pp. 711-728 (1988).

22. Y. Katto, "A physical approach to critical heat flux of subcooled flow boiling in round tubes," *International Journal of Heat and Mass Transfer*, **33**, No. 4, pp. 611-620 (1990).

23. G. P. Celata, M. Cumo, A. Mariani, M. Simoncini and G. Zummo, "Rationalization of existing mechanistic models for the prediction of water subcooled flow boiling critical heat flux," *International Journal of Heat and Mass Transfer* , **37**, suppl. 1, pp. 347-360 (1994).

24. S. S. Kutateladze, "Heat Transfer in Condensation and Boiling," AEC-tr-3770, USAEC (1959).

25. N. Zuber, "Hydrodynamic Aspects of Boiling Heat Transfer," AECU-4439, USAEC (1959).

26. A. Sakurai, M. Shiotsu, K. Hata and K. Fukuda, "Photographic study on transitions from non-boiling and nucleate boiling regime to film boiling due to increasing heat inputs in liquid nitrogen and water," *Nuclear Engineering and Design*, **200**, pp. 39-54 (2000).

27. T. Sato, and H. Matsumura, "On the Conditions of Incipient Subcooled-Boiling with Forced Convection," *Bulletin of JSME*, **7**, pp. 392-398 (1963).

28. A. E. Bergles, and W. M. Rohsenow, "The Determination of Forced-Convection Surface-Boiling Heat Transfer," *Journal of Heat Transfer*, Trans. ASME, Series C, **86**, pp. 365-372 (1964).

29. W. M. Rohsenow, "A Method of Correlating Heat-Transfer Data for Surface Boiling of Liquids," Transactions of ASME, **74**, pp. 969-976 (1952).

30. F. W. Dittus and L. M. K. Boelter, *Univ. Calif. (Berkeley) Pub. Eng.*, **2**, p. 443 (1930).

31. W. Nusselt, Der Wärmeaustausch zweischen Wand und Wasser im Rohr, *Forsch. Geb. Ingenieurwes.*, **2**, p. 309 (1931).

32. E. N. Sieder and C. E. Tate, "Heat Transfer and Pressure Drop of Liquids in Tubes," *Ind. Eng. Chem.*, **28**, pp. 1429-1435 (1936).

33. B. S. Petukhov, "Heat Transfer and Friction in Turbulent Pipe Flow with Variable Physical Properties," *Advances in Heat Transfer*, New York, Academic Press, pp. 503-564 (1970).

34. V. Gnielinski, "New Equations for Heat and Mass Transfer in Turbulent Pipe and Channel Flow," *International Chemical Engineering*, **16**, No. 2, pp. 359-368, (1976).

35. D. D. Hall, and I. Mudawar, "Ultra-high Critical Heat Flux (CHF) for Subcooled Water Flow Boiling-II: high-CHF Database and Design Equation," *International Journal of Heat and Mass Transfer*, **42**, pp. 1429-1456 (1999).

36. M. M. Shah, “Improved General Correlation for Critical Heat Flux during Upflow in Uniformly Heated Vertical Tubes,” *International Journal of Heat and Fluid Flow*, **8**, pp. 326-335 (1987).

37. S. M. Ghiaasiaan, “Two-Phase Flow, Boiling, and Condensation in Conventional and Miniature Systems,” Cambridge University Press, p. 381 (2008).

Table 1 Comparison of measured CHFs with CHF values derived from Celata et. al.'s liquid sub-layer dry-out model [23].

No	d (mm)	L (mm)	$\Delta T_{sub,in}$ (K)	P_{in} (kPa)	$\Delta T_{sub,out}$ (K)	P_{out} (kPa)	$(q_{cr,sub,st})_{exp}$ (W/m^2)	τ (s)	u (m/s)	$(q_{cr,sub,st})_{Celata\ Model}$ (W/m^2)	error (%)
8321	6	59.5	150.65	856.82	113.83	839.03	14.647	7.02	3.947	17.9724	-18.5028
8325	6	59.5	148.53	818.78	120.48	817.86	19.783	8.21	7.037	22.1431	-10.6584
8329	6	59.5	148.93	862.58	123.52	838.68	24.586	8.336	9.973	25.7272	-4.43577
8332	6	59.5	147.48	857.09	123.34	834.2	29.154	8.427	13.401	29.1324	0.074144
8337	6	59.5	148.17	871.42	124.94	829.3	32.866	8.497	17.171	33.165	-0.90155
8341	6	59.5	146.76	892.69	123.76	831.58	38.687	8.237	21.223	36.5028	5.983651
8347	6	59.5	141.85	942.03	116.33	820.28	51.354	7.883	30.634	40.9649	25.36098

Table 2 Comparison of measured CHFs with CHF values derived from authors' correlations, Eqs. (2) and (3), and Celata et. al.'s liquid sub-layer dry-out model [23], Hall and Mudawar correlation, Eq. (32), [35] and Shah correlation for LCC version, Eq. (34), [36, 37].

No	$\Delta T_{sub,in}$ (K)	$T_{sat,in}$ (K)	P_{in} (kPa)	$\Delta T_{sub,out}$ (K)	$T_{sat,out}$ (K)	P_{out} (kPa)	$q_{cr,exp}$ (W/m^2)	τ (s)	u (m/s)	d (mm)	L (mm)	$q_{cr,hata}$ (W/m^2)	error	error (%)	$q_{cr,celata}$ (W/m^2)	error	error (%)	$q_{cr,mudawar}$ (W/m^2)	error	error (%)	$q_{cr,shah}$ (W/m^2)	error	error (%)
8286	141.66	442.79	785.01	113.37	443.78	804.25	14.205	7.833	4.45	6	59.5	17.3037	0.8209	−17.91	18.4064	0.7717	−22.83	17.6992	0.8026	−19.74	19.6468	0.723	−27.7
8286	141.92	442.84	785.99	109.56	443.55	799.6	14.907	7.896	4.34	6	59.5	16.7378	0.8906	−10.94	17.7006	0.8422	−15.78	16.9621	0.8788	−12.12	19.2563	0.7741	−22.59
8290	145.52	447.3	874.59	117.08	445.86	845.11	18.961	8.13	7	6	59.5	21.0952	0.8988	−10.12	21.3922	0.8864	−11.37	22.9811	0.8251	−17.49	22.501	0.8427	−15.73
8291	144.44	447.19	872.38	115.11	445.63	840.55	19.631	8.164	6.99	6	59.5	20.8436	0.9418	−5.82	21.0285	0.9335	−6.65	22.6362	0.8672	−13.28	22.3167	0.8797	−12.03
8293	144.06	445.22	832.34	119.97	444.26	813.45	22.534	8.265	9.96	6	59.5	24.8099	0.9083	−9.17	25.0468	0.8997	−10.03	28.4582	0.7918	−20.82	25.2013	0.8942	−10.58
8294	144.15	445.15	830.95	118.87	444.2	812.4	23.213	8.295	9.94	6	59.5	24.6333	0.9423	−5.77	24.7967	0.9361	−6.39	28.2015	0.8231	−17.69	25.0663	0.9261	−7.39
8297	142.56	446.43	856.84	120.4	444.88	825.64	27.509	8.384	13.47	6	59.5	28.0195	0.9818	−1.82	28.524	0.9644	−3.56	33.4303	0.8229	−17.71	29.0064	0.9484	−5.16
8298	144.06	447.04	869.32	119.75	445.21	832.3	29.183	8.408	13.45	6	59.5	27.8744	1.0469	4.69	28.3268	1.0302	3.02	33.2094	0.8788	−12.12	28.9145	1.0093	0.93
8301	147.01	446.03	848.75	125.97	443.88	806.01	32.116	8.472	17.15	6	59.5	32.7618	0.9803	−1.97	33.5212	0.9581	−4.19	39.6867	0.8092	−19.08	33.2364	0.9663	−3.37
8302	147.03	446.13	850.72	123.93	444	808.44	33.191	8.487	17.14	6	59.5	32.3677	1.0254	2.54	32.9497	1.0073	0.73	39.0852	0.8492	−15.08	32.9518	1.0073	0.73
8305	146.06	447.64	881.83	123.3	444.54	818.92	38.051	8.189	21.35	6	59.5	35.9488	1.0585	5.85	36.5318	1.0416	4.16	43.6323	0.8721	−12.79	39.262	0.9692	−3.08
8306	144.48	447.6	881.03	122.99	444.56	819.3	38.43	8.186	21.36	6	59.5	35.8888	1.0708	7.08	36.4425	1.0545	5.45	43.539	0.8827	−11.73	39.2228	0.9798	−2.02
8311	142.19	450.33	939.21	120.05	444.34	814.97	47.531	8.318	30.79	6	59.5	42.3897	1.1213	12.13	42.4277	1.1203	12.03	51.7734	0.9181	−8.19	52.1688	0.9111	−8.89
8312	141.45	450.06	933.31	117.98	444.1	810.22	48.745	8.33	30.64	6	59.5	41.8014	1.1661	16.61	41.6135	1.1714	17.14	50.8964	0.9577	−4.23	51.5496	0.9456	−5.44
8313	142.21	450.36	939.79	118.73	444.44	817.02	47.961	8.326	30.77	6	59.5	42.0443	1.1407	14.07	41.9315	1.1438	14.38	51.2422	0.936	−6.4	51.8742	0.9246	−7.54
8314	141.64	451.18	957.96	117.33	445.22	832.44	51.059	7.817	30.66	6	59.5	41.539	1.2292	22.92	41.2824	1.2368	23.68	50.4757	1.0116	1.16	51.3919	0.9935	−0.65
8320	149.96	446.11	850.3	114.09	445.18	831.66	14.604	7.036	4.02	6	59.5	16.6189	0.8788	−12.12	18.0844	0.8075	−19.25	16.7736	0.8707	−12.93	19.2052	0.7604	−23.96
8321	150.65	446.43	856.82	113.83	445.55	839.03	14.647	7.02	3.95	6	59.5	16.4608	0.8898	−11.02	17.9724	0.815	−18.50	16.5648	0.8842	−11.58	19.1097	0.7665	−23.35
8322	149.37	444.94	826.8	126.54	444.64	820.97	18.513	7.088	7.01	6	59.5	22.3526	0.8282	−17.18	23.2306	0.7969	−20.31	24.7271	0.7487	−25.13	23.3036	0.7944	−20.56
8324	148.24	445.7	841.92	122.17	445.14	830.88	18.504	8.149	7.07	6	59.5	21.864	0.8463	−15.37	22.4561	0.824	−17.60	24.0498	0.7694	−23.06	22.9096	0.8077	−19.23
8325	148.53	444.53	818.78	120.48	444.49	817.86	19.783	8.21	7.04	6	59.5	21.6432	0.9141	−8.59	22.1431	0.8934	−10.66	23.7436	0.8332	−16.68	22.7432	0.8698	−13.02
8327	148.21	445.3	834.03	124.82	445.3	834.03	22.351	8.292	9.98	6	59.5	25.4661	0.8777	−12.23	26.0285	0.8587	−14.13	29.4072	0.7601	−23.99	25.7189	0.8691	−13.09
8328	148.4	445.15	831.01	123.45	445.15	831.01	23.074	8.294	9.98	6	59.5	25.2804	0.9127	−8.73	25.7501	0.8961	−10.39	29.1379	0.7919	−20.81	25.5828	0.9019	−9.81
8329	148.93	446.71	862.58	123.52	445.53	838.68	24.586	8.336	9.97	6	59.5	25.2541	0.9735	−2.65	25.7272	0.9556	−4.44	29.0967	0.845	−15.5	25.5774	0.9612	−3.88
8331	148.07	447.19	872.48	125.37	445.83	844.65	27.66	8.405	13.42	6	59.5	28.7141	0.9633	−3.67	29.5983	0.9345	−6.55	34.4698	0.8024	−19.76	29.5327	0.9366	−6.34
8332	147.48	446.44	857.09	123.34	445.31	834.2	29.154	8.427	13.4	6	59.5	28.4091	1.0262	2.62	29.1324	1.0007	0.07	34.0108	0.8572	−14.28	29.279	0.9957	−0.43
8336	147.66	446.89	866.24	125.97	444.92	826.45	31.719	8.505	17.17	6	59.5	32.6941	0.9702	−2.98	33.4511	0.9482	−5.18	39.5643	0.8017	−19.83	33.2331	0.9544	−4.56
8337	148.17	447.14	871.42	124.94	445.06	829.3	32.866	8.497	17.17	6	59.5	32.4981	1.0113	1.13	33.165	0.991	−0.90	39.2624	0.8371	−16.29	33.1021	0.9929	−0.71
8340	146.14	447.89	886.87	123.38	444.77	823.4	37.62	8.22	21.23	6	59.5	35.8483	1.0494	4.94	36.4349	1.0325	3.25	43.4988	0.8649	−13.51	39.0956	0.9623	−3.77
8341	146.76	448.16	892.69	123.76	445.18	831.58	38.687	8.237	21.22	6	59.5	35.8802	1.0782	7.82	36.5028	1.0598	5.98	43.5442	0.8885	−11.15	39.1244	0.9888	−1.12
8345	146.01	450.43	941.36	119.17	444.55	819.03	49.642	7.85	30.66	6	59.5	42.0657	1.1801	18.01	42.015	1.1815	18.15	51.2922	0.9678	−3.22	51.8077	0.9582	−4.18
8346	141.35	450.05	933.1	117.7	443.92	806.91	49.585	7.853	30.8	6	59.5	41.8557	1.1847	18.47	41.6194	1.1914	19.14	50.9563	0.9731	−2.69	51.7112	0.9589	−4.11
8347	141.85	450.45	942.03	116.33	444.61	820.28	51.354	7.883	30.63	6	59.5	41.3367	1.2423	24.23	40.9649	1.2536	25.36	50.1777	1.0234	2.34	51.1782	1.0034	0.34
8440	159.03	446.15	850.97	114.33	445.19	831.87	17.377	7.965	4.05	6	59.7	16.6985	1.0406	4.06	18.1521	0.9573	−4.27	16.886	1.0291	2.91	19.2477	0.9028	−9.72
8441	156.9	445.18	831.57	129.59	444.74	822.94	18.751	8.076	7.02	6	59.7	22.7346	0.8248	−17.52	23.8093	0.7875	−21.25	25.2739	0.7419	−25.81	23.5539	0.7961	−20.39
8444	154.95	445.97	847.57	130.97	445.1	830.16	23.807	8.243	10.01	6	59.7	26.3727	0.9027	−9.73	27.3742	0.8697	−13.03	30.7523	0.7742	−22.58	26.3397	0.9038	−9.62
8445	150.97	445.63	840.53	129.75	445.19	831.78	25.017	8.248	10.01	6	59.7	26.1874	0.9553	−4.47	27.1022	0.9231	−7.69	30.4782	0.8208	−17.92	26.2112	0.9544	−4.56
8448	154.6	446.91	866.61	130.87	445.57	839.46	29.784	8.301	13.38	6	59.7	29.5634	1.0075	0.75	30.8905	0.9642	−3.58	35.7758	0.8325	−16.75	30.0873	0.9899	−1.01
8449	154.61	447.09	870.29	131.2	445.49	837.8	29.022	8.301	13.37	6	59.7	29.6107	0.9801	−1.99	30.963	0.9373	−6.27	35.8482	0.8096	−19.04	30.1116	0.9638	−3.62
8452	155.2	446.64	860.92	134.05	444.31	814.53	30.887	8.357	17.12	6	59.7	34.1409	0.9047	−9.53	35.6321	0.8668	−13.32	41.8317	0.7384	−26.16	34.1719	0.9039	−9.61
8453	154.74	447.01	868.56	134.41	444.68	821.69	32.354	8.377	17.15	6	59.7	34.2014	0.946	−5.4	35.7241	0.9057	−9.43	41.9119	0.772	−22.8	34.2513	0.9446	−5.54
8455	156.3	448.52	900.15	133.78	445.24	832.88	36.65	8.123	21.16	6	59.7	37.8173	0.9691	−3.09	39.4356	0.9294	−7.06	46.5675	0.787	−21.3	40.5079	0.9048	−9.52
8456	156.3	448.07	890.81	133	444.66	821.43	36.942	8.126	21.16	6	59.7	37.7117	0.9796	−2.04	39.253	0.9411	−5.89	46.4152	0.7959	−20.41	40.4028	0.9143	−8.57
8461	153.01	451.21	958.66	128.84	444.43	816.88	49.171	7.768	30.56	6	59.7	44.3523	1.1086	10.86	45.4733	1.0813	8.13	54.8821	0.8959	−10.41	53.6104	0.9172	−8.28
8462	152.5	451.26	959.58	127.55	444.61	820.24	50.604	7.791	30.55	6	59.7	44.0171	1.1496	14.96	44.982	1.125	12.50	54.3559	0.931	−6.9	53.3297	0.9489	−5.11
8463	154.37	451.58	966.89	128.05	445.17	831.35	49.854	7.785	30.55	6	59.7	44.0773	1.1311	13.11	45.1041	1.1053	10.53	54.4387	0.9158	−8.42	53.4067	0.9335	−6.65
8464	153.56	451.55	966.14	125.12	444.71	822.26	52.447	7.863	30.56	6	59.7	43.4205	1.2079	20.79	44.0926	1.1895	18.95	53.424	0.9817	−1.83	52.8358	0.9926	−0.74

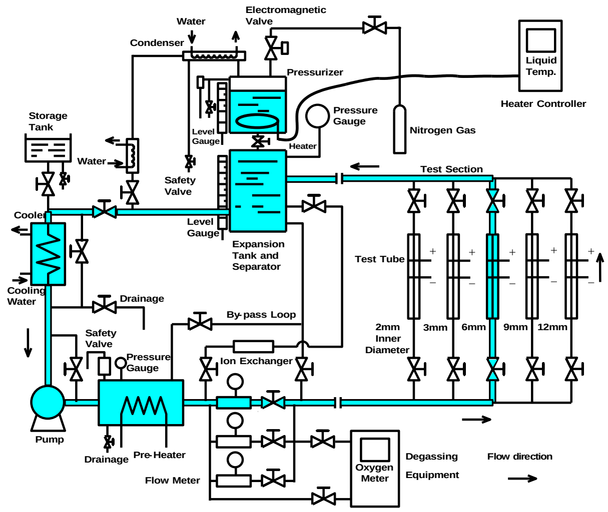

Fig. 1 Schematic diagram of experimental water loop.

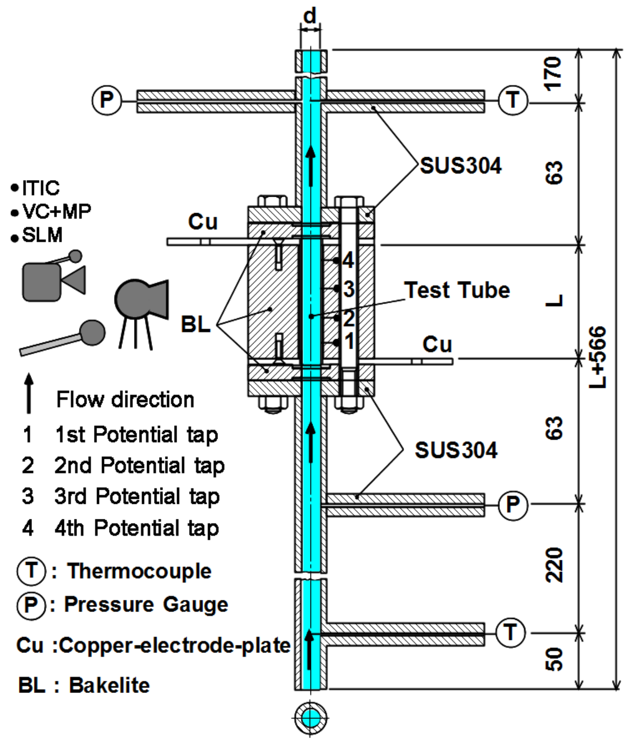

Fig. 2 Vertical cross-sectional view of 6-mm inner diameter test section.

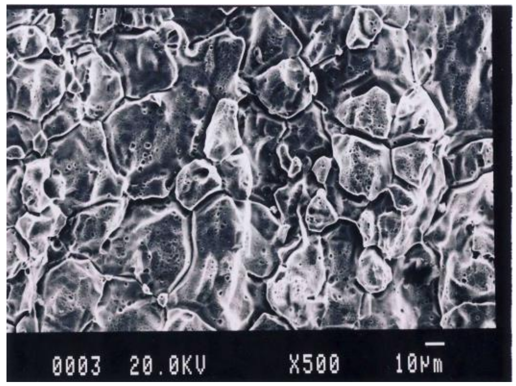

Fig. 3 SEM photograph for the SUS304 test tube of d=6 mm with the rough finished inner surface.

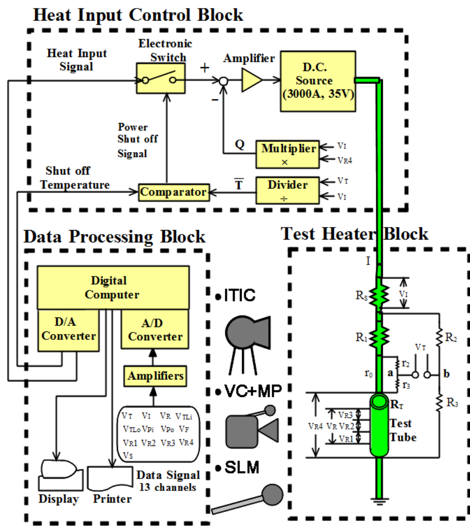

Fig. 4 Measurement and data processing system.

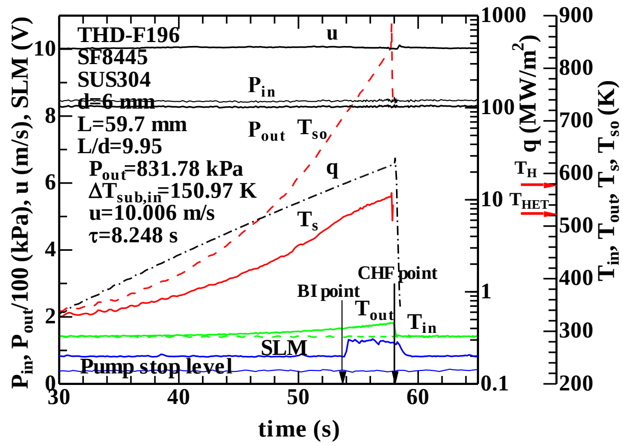

Fig. 5 Typical time variations in P_{in}, P_{out}, q, T_s, T_{so}, T_{in}, T_{out}, u and SLM signals for P_{out}=831.8 kPa, $\Delta T_{sub,in}$=150.9 K, u=10.0 m/s and τ=8.25 s.

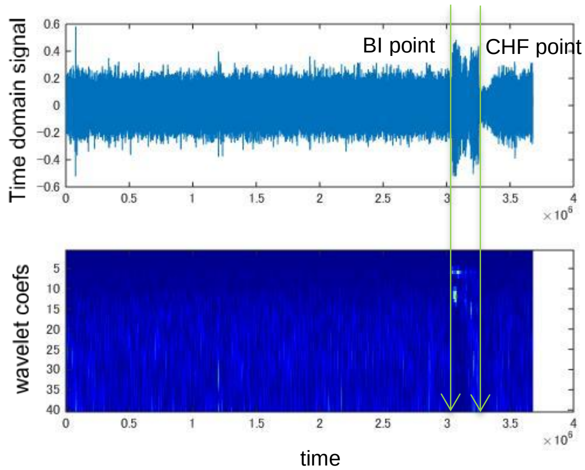

Fig. 6 Typical time domains in MP signals and the contour of various wavelet coefficients for P_{out}=831.8 kPa, $\Delta T_{sub,in}$=150.9 K, u=10.0 m/s and τ=8.25 s.

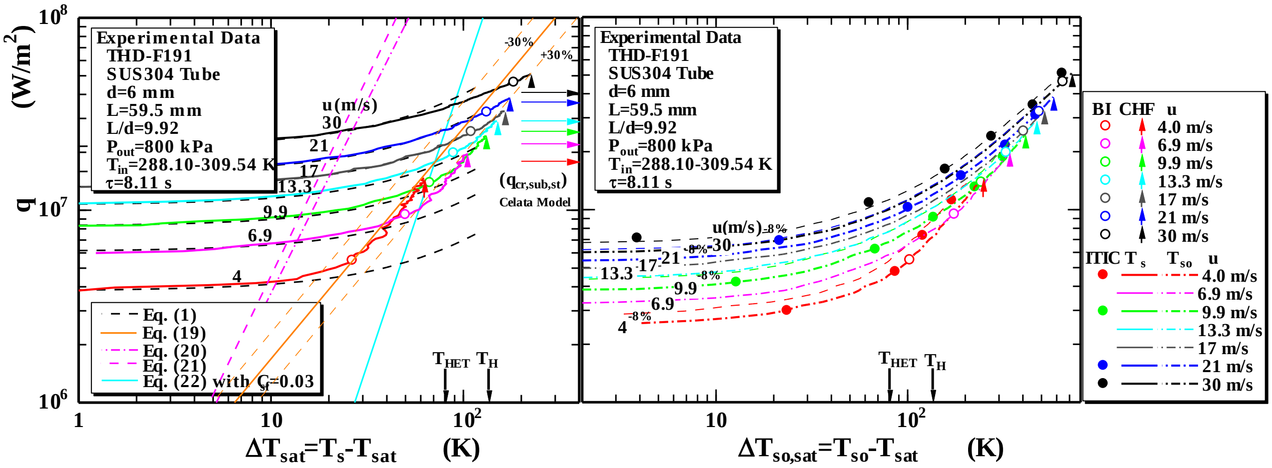

Fig. 7 Typical heat transfer processes on the THD-F191 SUS304 test tube of d=6 mm and L=59.5 mm with the rough finished inner surface for τ=around 8.02 s with u=4 to 30 m/s, and outer surface temperatures of the test tube calculated from Eq. (14) and observed by an infrared thermal imaging camera (ITIC).

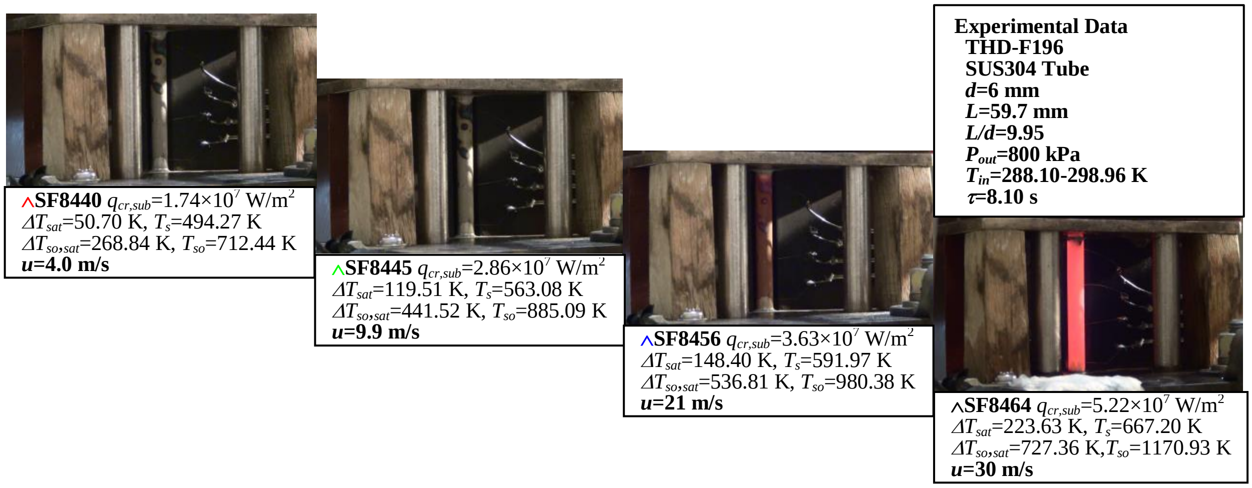

Fig. 8 Typical photographs for color temperatures of outer surface of the test tube at CHF point observed by a video camera (VC).

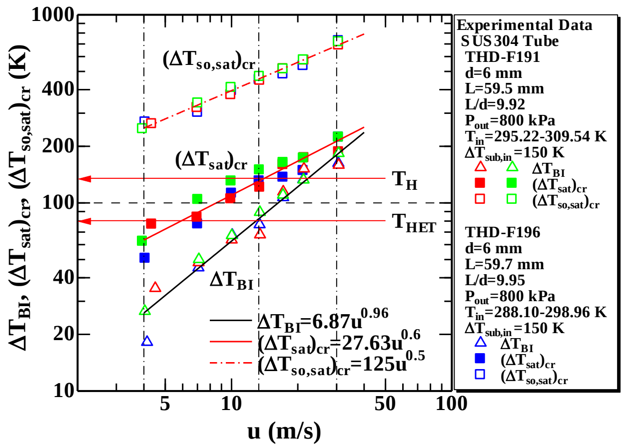

Fig. 9 Values of ΔT_{BI}, $(\Delta T_{sat})_{cr}$ and $(\Delta T_{so,sat})_{cr}$ versus u for vertical SUS304 test tubes of d=6 mm.

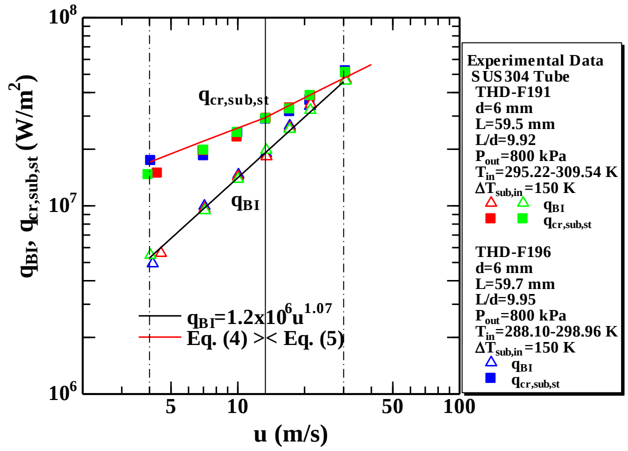

Fig. 10 Values of q_{BI} and $q_{cr,sub,st}$ versus u for vertical SUS304 test tubes of d=6 mm.

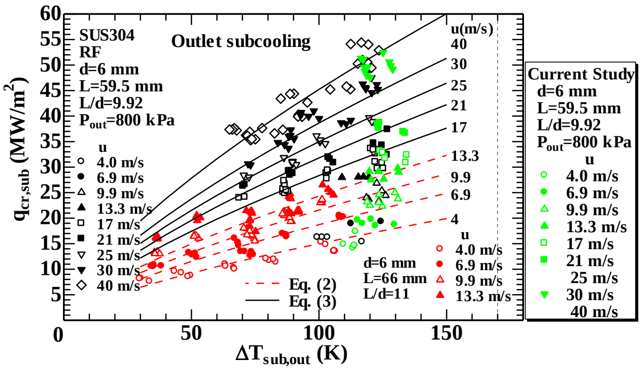

Fig. 11 $q_{cr,sub,st}$ vs. $\Delta T_{sub,out}$ for an inner diameter of 6 mm with the heated length of 59.5 mm at an outlet pressure of around 800 kPa.

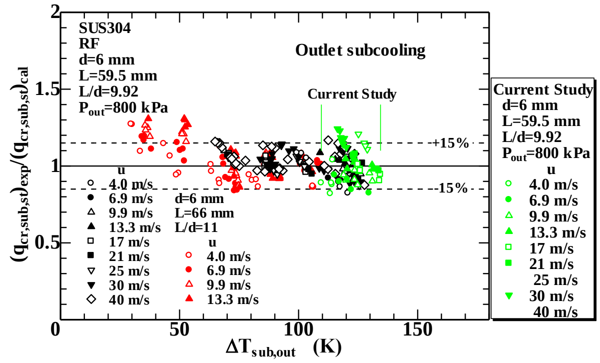

Fig. 12 Ratios of CHF data for the inner diameter of 6 mm to the values derived from the outlet CHF correlation versus $\Delta T_{sub,out}$ at outlet pressure of around 800kPa.

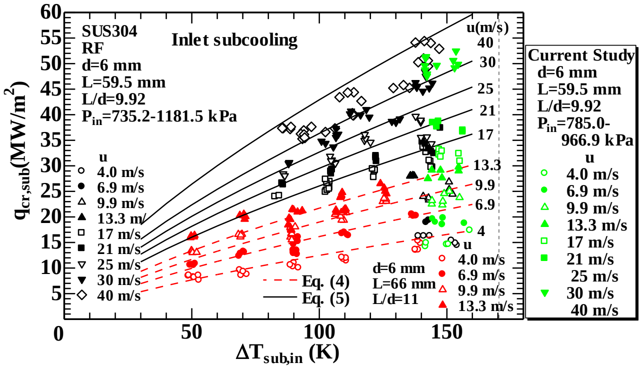

Fig. 13 $q_{cr,sub,st}$ vs. $\Delta T_{sub,in}$ for an inner diameter of 6 mm with the heated length of 59.5 mm at an inlet pressures of 785.01 to 966.89 kPa.

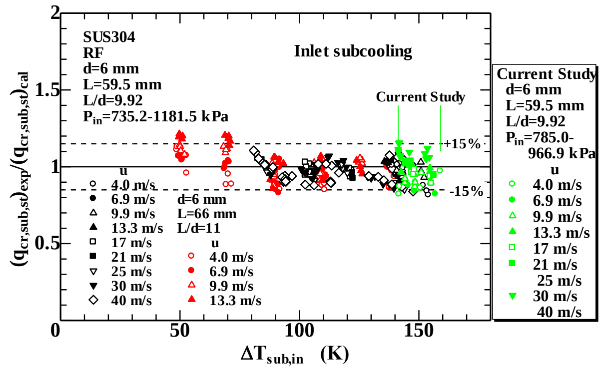

Fig. 14 Ratios of CHF data for the inner diameter of 6 mm to the values derived from the inlet CHF correlation versus $\Delta T_{sub,in}$ at the inlet pressures of 785.01 to 966.89 kPa.

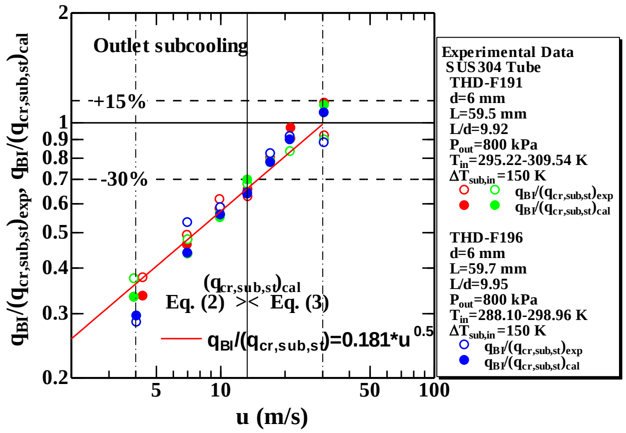

Fig. 15 Ratios of BI data for the inner diameter of 6 mm to the CHF data and the values derived from the outlet CHF correlation versus *u* at outlet pressure of around 800kPa.

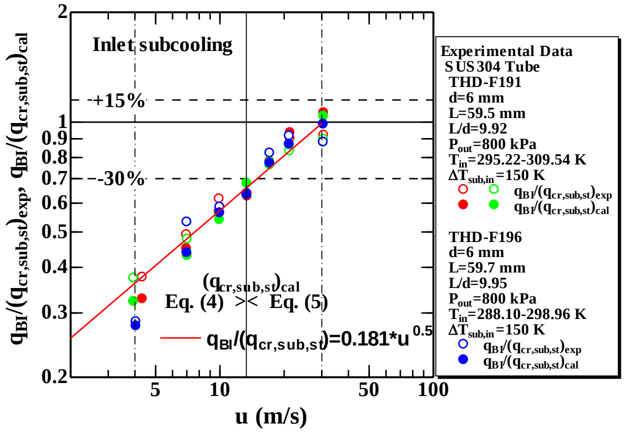

Fig. 16 Ratios of BI data for the inner diameter of 6 mm to the CHF data and the values derived from the inlet CHF correlation versus *u* at the inlet pressures of 785.01 to 966.89 kPa.

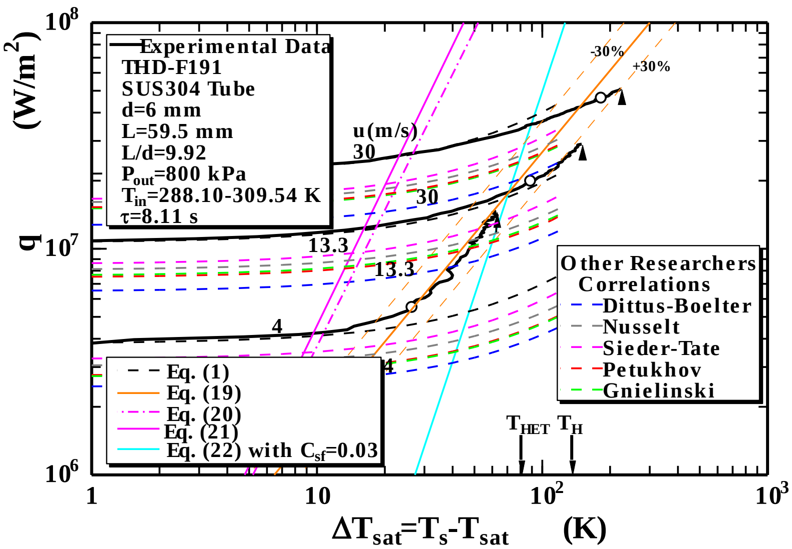

Fig. 17 Typical heat transfer processes on the THD-F191 SUS304 test tube of d=6 mm and L=59.5 mm with the rough finished inner surface for τ=around 8.02 s with u=4, 13.3 and 30 m/s and the values calculated from Dittus-Boelter, Nusselt, Sieder-Tate, Petukhov and Gnielinski correlations.

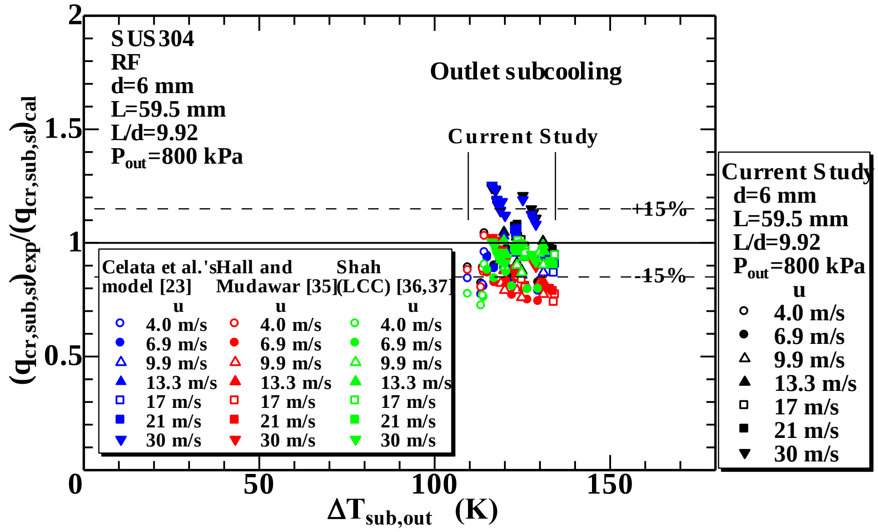

Fig. 18 Comparison of CHF data for the THD-F191 SUS304 test tube of d=6 mm and L=59.5 mm with the rough finished inner surface with authors' correlations, Eqs. (2) and (3), solutions of Celata et. al.'s liquid sub-layer dry-out model [23], Hall and Mudawar correlation, Eq. (33), [35] and Shah correlation for LCC version, Eq. (34), [36, 37].